Title

Inhomogeneous Knight shift in vortex cores of superconducting FeSe

Permalink

https://escholarship.org/uc/item/0qg1w2gc

Authors

Vinograd, I
Edwards, SP
Wang, Z
et al.

Publication Date

2021-02-17

Peer reviewed

Inhomogeneous Knight shift in vortex cores of superconducting FeSe

I. Vinograd,[1] S. P. Edwards,[1] Z. Wang,[1] T. Kissikov,[1] J. K. Byland,[1] J. R. Badger,[2] V. Taufour,[1] and N. J. Curro[1]

[1]*Department of Physics and Astronomy, University of California, Davis, California 95616, USA*
[2]*Department of Chemistry, University of California, Davis, California 95616, USA*
(Dated: February 19, 2021)

We report ^{77}Se NMR data in the normal and superconducting states of a single crystal of FeSe for several different field orientations. The Knight shift is suppressed in the superconducting state for in-plane fields, but does not vanish at zero temperature. For fields oriented out of the plane, little or no reduction is observed below T_c. These results reflect spin-singlet pairing emerging from a nematic state with large orbital susceptibility and spin-orbit coupling. The spectra and spin-relaxation rate data reveal electronic inhomogeneity that is enhanced in the superconducting state, possibly arising from enhanced density of states in the vortex cores. Despite the spin polarization of these states, there is no evidence for antiferromagnetic fluctuations.

The iron-based superconductors have attracted broad interest recently because they can host Majorana modes on the surface, at domain walls, and within vortex cores [1–4]. Fe(Se,Te), and Li(Fe,Co)As contain bands with p_z and d_{xz}/d_{yz} character with non-trivial topologies, that give rise to both topological surface states as well as a bulk Dirac point near the Γ point in k-space [5]. FeSe, although topologically trivial, is a particularly interesting case because the superconducting state emerges from a nematic phase that develops below $T_{nem} = 91$K [6]. Moreover, the Fermi energy, E_F, in this system is usually small, such that this system lies close to the BCS-BEC crossover regime [7, 8]. Evidence has emerged that suggests FeSe exhibits a Fulde-Ferell-Larkin-Ovchinnikov (FFLO) phase at high magnetic fields [9]. The possibility of both FFLO and dispersive Majorana modes underlies the importance of a detailed understanding of the nature of the vortices in these materials.

To probe vortex matter it is important to first understand the underlying superconducting state. The spatial part of the superconducting wavefunction in FeSe is generally assumed to be either $s_\pm$ or d-wave. The nematic normal state gives rise to twin domains and in-plane anisotropy, and the Fermi surfaces contain different orbital characters in the two domains. The superconducting gap, Δ, appears to correlate with the orbital content on the Fermi surface [10]. However, the presence of the domains may mask intrinsic properties about the density of states below T_c, and there are conflicting reports about the presence or lack of nodes and anisotropy of the superconducting gap function [11–14].

Information about the spin component of the wavefunction can be gleaned from nuclear magnetic resonance (NMR) Knight shift measurements. The spin susceptibility of a condensate with singlet pairing vanishes, whereas that with triplet pairing can remain unchanged through T_c. Conventional magnetometry cannot discern these changes because the spin component is much smaller than the orbital component, however the Knight shift is usually dominated by the former and is thus one of the only experimental probes of the spin susceptibility of the con-
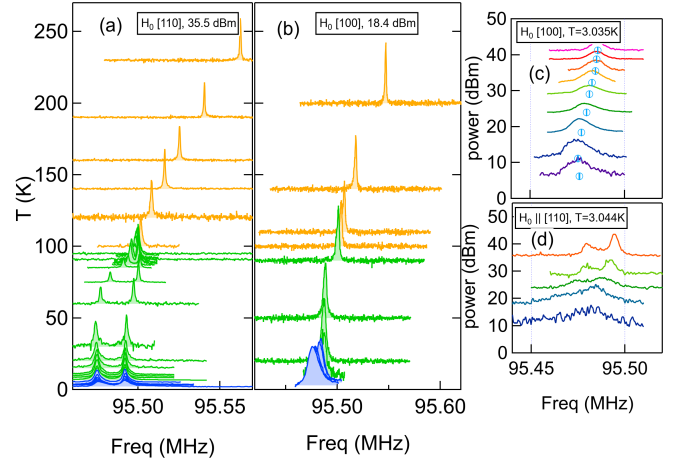

FIG. 1. (a) ^{77}Se NMR spectra (normalized) as a function of temperature for $\mathbf{H}_0 \parallel [110]$ (in tetragonal unit cell) at high rf power (35.5 dBm). Below $T_{nem} = 91$K, the single resonance splits into two separate peaks, corresponding to domains with $\mathbf{H}_0 \parallel \mathbf{a}$ (upper peak) and $\mathbf{H}_0 \parallel \mathbf{b}$ (lower peak) in the nematic phase. (b) Spectra as a function of temperature for $\mathbf{H}_0 \parallel [110]$ at low rf power (18.4 dBm). (c,d) Spectra in the superconducting state as a function of radiofrequency pulse power for $\mathbf{H}_0 \parallel [100]$ and $\mathbf{H}_0 \parallel [110]$, respectively. Blue circles in (c) indicate the first moment of the spectrum.

densate [7, 8]. To date, Knight shift measurements in the superconducting state have been inconclusive, revealing little or no change below T_c [15–18]. A recent study reported no change in the Knight shift along the c axis in fields up to 16 T, which have been interpreted as evidence for highly spin-polarized Fermi liquid in the BCS-BEC regime [19]. A lack of suppression of the Knight shift may be evidence for spin-triplet pairing [20], but may also reflect thermal instability of the sample due to eddy-current heating from radiofrequency pulses [21]. In fact, spin-orbit coupling can give rise naturally to a spin-triplet component [22, 23]. To fully characterize the symmetry of the condensate, therefore, it is important to understand the full tensor nature of the Knight shift in

the superconducting state.

Here we report ^{77}Se NMR on a high quality single crystal as a function of temperature and field. We find that between 3.6 and 11.7 T, the spin part of the planar Knight shift is reduced by $\sim 10-15\%$ from their normal state values below T_c, whereas the out-of-plane component shows no change within the experimental resolution. These results are consistent with spin singlet pairing in the presence of large orbital susceptibility and spin-orbit coupling. Surprisingly, the NMR linewidths broaden inhomogenously by more than a factor of two below T_c for planar fields, but not for $\mathbf{H}_0 \parallel \mathbf{c}$. Accompanying this broadening is a frequency-dependent spin-lattice relaxation rate, T_1^{-1}, that reveals electronic inhomogeneity in the superconducting state. This inhomogeneity cannot be explained by the presence of a conventional vortex lattice, but may reflect an enhanced local density of states within the vortex cores.
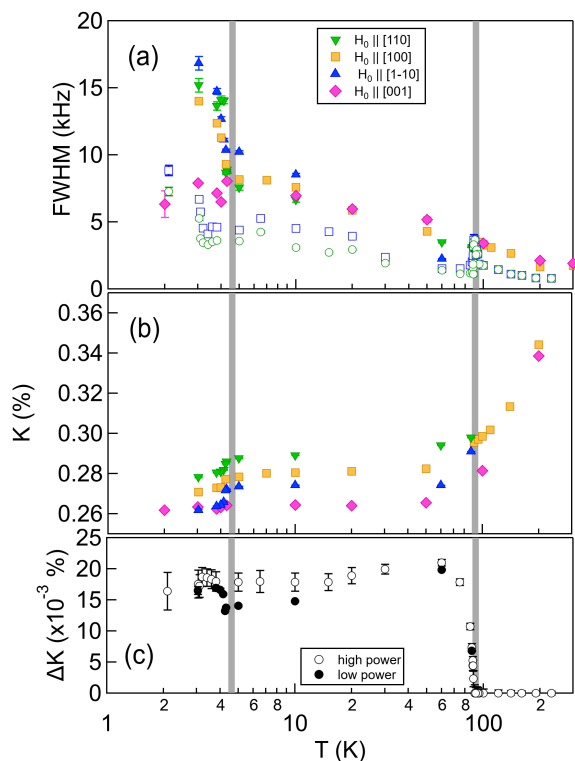

FIG. 2. Linewidth (a) and Knight shifts (b) of the spectra in Fig. 1 as a function of temperature for the field along $[110] \sim \mathbf{a}$ (▼), $[1\bar{1}0] \sim \mathbf{b}$ (▲), $[100]$ (■), and $[001] \sim \mathbf{c}$ (♦). (c) The in-plane anisotropy $\Delta K = K_a - K_b$ as a function of temperature. Solid (open) points were acquired at low (high) rf power, respectively, as discussed in the text.

Single crystals of FeSe were grown by vapor transport with a tilted two-temperature zone tube furnace [24]. Several samples were characterized with magnetic sus-

ceptibility and resistivity measurements, with the best samples having $T_c = 8.9\,\mathrm{K}$, and RRR defined as the resistance ratio between 250 and $10\,\mathrm{K}$ around 19, similar to reported high-quality samples [24]. A large crystal of dimensions 2.4 mm $\times$1.4 mm $\times$ 0.2 mm was selected and mounted in a custom-built NMR probe equipped with a dual-axis goniometer. The majority of the experiments were conducted within a variable-temperature cryostat in a high-homogeneity NMR magnet with a field of $H_0 = 11.7294$ T, and some experiments at lower fields were conducted in a PPMS system. In this field, T_c is suppressed to ~ 5.3 K (measured by resistivity) [25]. Spectra (Fig. 1) were collected for field aligned along the tetragonal [110], [100] and [001] directions. The [110] ($[1\bar{1}0]$) direction corresponds to the Fe-Fe bond, and is the $\mathbf{a}$ ($\mathbf{b}$) direction in the nematic phase [26]. The spectra were measured at several temperatures down to 2.1 K using low-power rf pulses ($\pi/2$-pulse widths up to 80μs), sweeping frequency and summing the Fourier transforms. Our results are consistent with previous reports [15–18, 27], and reveal a splitting of the single ^{77}Se resonance below $T_{nem} = 91$ K due to twinning. The resonance frequencies are given by $f = \gamma H_0(1 + K)$, where $\gamma = 8.118$ MHz/T is the gyromagnetic ratio and K is the Knight shift. We fit each resonance to a Gaussian function, and Figs. 2(a,b) shows the temperature dependence of K and the full-width half-maxima, FWHM, for several different field directions. Below T_c, the spectra exhibited a strong dependence on the pulse power, as illustrated in Fig. 1(c,d). The radiofrequency pulses induce eddy currents around the sample, which can lead to Joule heating. As a result, the temperature may temporarily exceed T_c immediately after the pulse. Similar effects have been observed in other superconductors, leading to misinterpretations about the temperature dependence of the Knight shift [21]. The shifts reported in Fig. 2(b) were measured at 18.4 dBm, where there was no power-dependence to the spectra.

The Knight shift arises from the hyperfine interaction between the nuclear spin and the spin and orbital degrees of freedom of the electrons: $\mathcal{H}_{hf} = \mathbf{I} \cdot \mathbb{A}_S \cdot \mathbf{S} + \mathbf{I} \cdot \mathbb{A}_L \cdot \mathbf{L}$, where $\mathbb{A}_{S,L}$ are the hyperfine coupling tensors, and $\mathbf{S}$ and $\mathbf{L}$ are the spin and orbital angular momenta. The Knight shift is given by $K_\alpha = A^L_{\alpha\alpha}\chi^{orb}_{\alpha\alpha} + A^S_{\alpha\alpha}\chi^{spin}_{\alpha\alpha} + (A^S_{\alpha\alpha} + A^L_{\alpha\alpha})\chi^{mixed}_{\alpha\alpha}$, where $\chi^{spin}_{\alpha\alpha}$, $\chi^{orb}_{\alpha\alpha}$, and $\chi^{mixed}_{\alpha\alpha}$ are the static spin, orbital, and mixed susceptibilities at zero wavevector [26, 28]. In the absence of spin-orbit coupling, the mixed term vanishes and the Knight shift is usually decomposed as $K_\alpha = K_{\alpha0} + A^S_{\alpha\alpha}\chi^{spin}_{\alpha\alpha}$. $K_{\alpha0}$ is often considered to be a temperature-independent shift arising from a Van-Vleck orbital susceptibility, however, this decomposition breaks down in the presence of spin-orbit coupling [29]. Moreover, theoretical calculations have revealed that $\chi^{orb}_{\alpha\alpha} \gg \chi^{spin}_{\alpha\alpha}, \chi^{mixed}_{\alpha\alpha}$ due to the multiorbital nature of the band structure and nematic instability [26]. As a result, the relationship between K_α

and the bulk susceptibility, $\chi = \chi^{spin} + \chi^{orb} + 2\chi^{mixed}$, is complicated. Nevertheless, we find that K_α varies linearly with χ above T_{nem}, as shown in the inset of Fig. 3. Linear fits to the data yield parameters close to previously reported values [18].

For spin-singlet pairing, χ^{spin} and χ^{mixed} should vanish in the superconducting state, giving rise to a suppression of K below T_c, as observed in Fig. 3. For planar fields, $K_{a,b}$ is suppressed by about 100 ± 15 ppm in both domains, as well as for the [100] direction oriented $45°$ to the Fe-Fe bond direction. This magnitude of suppression does not change significantly at lower fields. For out of plane fields, any change in K_c is within the noise, but is less than ~ 10 ppm. These results are also independent of applied field, and are consistent with previous reports [19, 30]. Note that $K_\alpha(T \to 0) \neq K_{\alpha 0}$, or in other words the low temperature limit of the shift does not equal the intercepts from the $K - \chi$ plot. In fact, χ^{orb} is strongly temperature dependent, so $K_{\alpha 0}$ does not represent a temperature independent Van-Vleck term. The low temperature shift reflects a finite χ^{orb}, since the spin component vanishes for singlet pairing; however impurity states may play a role [31]. Determining how much χ^{spin}, χ^{orb} and χ^{mixed} are suppressed below T_c will likely require detailed theoretical calculations [26]. It is noteworthy that the difference $K_a - K_b$, shown in Fig. 2(c), exhibits a subtle enhancement below T_c. This observation suggests that the superconductivity is slightly anisotropic in the two domains, and may reflect an anisotropy in the coherence lengths, $\xi_{a,b}$.

Below T_c the spectra for both domains broaden and become asymmetric with a high frequency tail, as observed in Fig. 1(c,d) and 2(a). At room temperature, the FWHM of the spectrum (~ 0.08 kHz) is close to the second moment of the nuclear spin dipole moments of the lattice (~ 0.06 kHz). The excess inhomogeneous broadening above T_c may be due to either macroscopic or microscopic strain fields [32]. The crystals were initially secured to the goniometer with a light coat of superglue and the coil fit loosely around the sample. In this case, the observed linewidths were smaller (open points in Fig. 2(a)), reflecting the high quality of this crystal. In later measurements, the crystal was remounted and we observed the linewidth increase by a factor ~ 2 (solid points in Fig. 2(a)). It is possible that remounting the crystal introduced inhomogeneous macroscopic strain fields. Non-magnetic impurities such as Fe vacancies are known to exist in the lattice [10], which may also be a source of local strain and inhomogeneous broadening in the normal state.

Regardless of the linewidth in the normal state, an even larger increase of linewidth is observed below T_c, which is unexpected. A vortex lattice certainly gives rise to a distribution of local magnetic fields, $B(\mathbf{r})$, and in very low fields $B \ll B_{c2}$, the second moment of the field distribution can be estimated as $\Delta B^2 \approx 0.00371\phi_0^2\lambda^{-4}$,
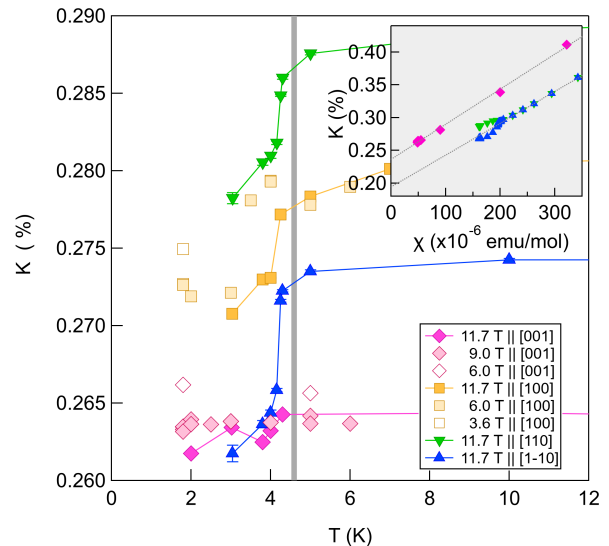

FIG. 3. K_α versus temperature for fields and orientations. (INSET) K versus χ for in the normal state, using susceptibility data from [18]. The dotted lines indicate the best linear fits, with parameters $K_{0a} = 0.194 \pm 0.002\%$, $A_{aa} = 27.1 \pm 0.3$ kOe/μ_B, $K_{0c} = 0.236 \pm 0.001\%$, and $A_{cc} = 29.9 \pm 0.5$ kOe/μ_B, as described in the text.

where ϕ_0 is the flux quantum, and the penetration depths are $\lambda_a = 446$ nm, $\lambda_c = 1320$ nm [33, 34]. There are important corrections to this expression in the higher fields where our measurements were conducted [35], however after accounting for these we estimate that the normal state spectra should broaden by only ~ 8 Hz, three orders of magnitude smaller than the enhancement observed in Fig. 2(a) [36].

Since the field distribution alone is unable to capture the asymmetric broadening, we hypothesize the presence of a spatially-varying Knight shift, $K_\alpha(\mathbf{r})$, that is equal to the normal state value within the vortex cores and decays to $K_\alpha(T \to 0)$ outside. The spectrum is given by the histogram of the local resonance frequency, $f(\mathbf{r}) = \gamma B(\mathbf{r})(1 + K_\alpha(\mathbf{r}))$. The exact shape of the spectrum depends on microscopic details, but if the spatial variation δK is equal to the 100 ppm suppression observed in Fig. 3, the spectrum will broaden by ~ 10 kHz, which agrees well with the excess linewidth below T_c in Fig. 2(a). These results suggest that the local spin susceptibility within the vortex cores is identical to that in the normal state.

This interpretation is supported by T_1^{-1} measurements. Fig. 4(a) shows $(T_1T)^{-1}$ versus temperature. The data in the normal state agree well with published results [15, 18, 37]. This quantity drops due to the superconductivity, and becomes inhomogeneous in the mixed phase. Fig. 4(b) shows that T_1^{-1} increases by nearly a factor of two in the high frequency tails of the spec-

tra in the superconducting state, which correspond with the vortex cores. Localized Caroli-deGennes-Matricon (CdGM) electronic states normally exist within isolated cores [38]. At higher fields quasiparticles from different cores can propagate coherently across multiple vortices, and the energy spectrum becomes dispersive, with gapless excitations remaining within the vortex cores that give rise to a finite local density of states (LDOS) which should be manifest in any technique sensitive to low energy excitations [39–42]. Indeed NMR studies have identified enhanced spin-lattice-relaxation rate within the vortex cores of both conventional [43] and unconventional superconductors [44, 45].
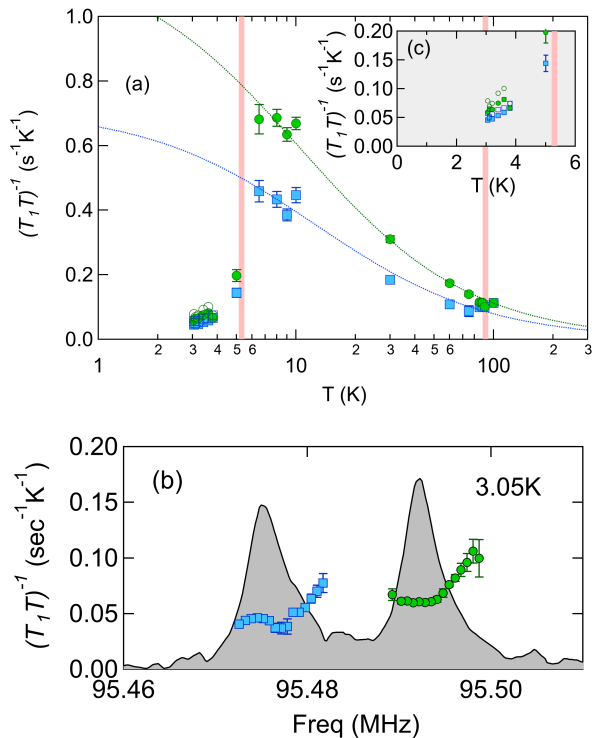

FIG. 4. (a) $(T_1T)^{-1}$ versus temperature (symbols defined in Fig. 2). The dotted lines are best fits to a Curie-Weiss form, as described in the text. (b) $(T_1T)^{-1}$ versus frequency at 3.05K in the mixed phase, revealing an enhanced rate within the vortex cores. The spectrum is shown in gray. T_1^{-1} and spectra were acquired with high power rf pulses.

There are, however, important differences between FeSe and previous observations on other superconductors. In the cuprates, the excess relaxation rate has been attributed to antiferromagnetic fluctuations from a competing ground state to superconductivity [44, 45], as well as from Doppler-shifted quasiparticles associated with d-wave nodes [46]. In such cases $(T_1T)^{-1}$ exhibits a strong Curie-Weiss divergence within the cores, whereas outside the cores $(T_1T)^{-1}$ remains temperature independent. In the s-wave superconductor $LaRu_4P_{12}$, $(T_1T)^{-1}$ in the

cores is also strongly temperature dependent, and even exceeds the value in the normal state [43]. In the case of FeSe, $(T_1T)^{-1}$ exhibits Curie-Weiss behavior in the normal state (dotted lines in Fig. 4a), but drops below T_c. This behavior has been attributed to antiferromagnetic spin fluctuations that are gapped by the superconductivity [47, 48]. The open circles (squares) in Fig. 4(a,c) show the temperature dependence at the upper end of the spectra in the superconducting state. $(T_1T)^{-1}$ in the vortex cores changes only by a factor of two from the background rate, remaining well below the normal state value, and exhibits the same trend with temperature as the background. These results suggest the absence of any spin fluctuations within the normal cores of FeSe.

FeSe appears unique in that there is a $\mathbf{q} = 0$ spin response in the vortex cores. It is unclear whether this behavior could be related to either a proximity to the BCS-BEC crossover, or either a Fulde-Ferrell-Larkin-Ovchinnikov (FFLO) phase [8, 9] or a field-induced spin density wave [49] for parallel fields above $H^* = 24$ T. A true FFLO phase should exhibit both segmented vortex lines and normal planes where the LDOS reaches the normal state values, giving rise to inhomogeneously broadened NMR spectra. Although $H_0 \sim 0.5H^*$ in our experiments, the inhomogeneity we observe already indicates the presence of large spin polarization in spatial regions where the superconducting order vanishes. It is noteworthy that the $\mathbf{q} = 0$ susceptibility in FeSe is dominated by orbital contributions, whereas the finite $\mathbf{q}$ response is dominated by spin fluctuations [26]. Condensation of singlet pairs enables us to probe the small spin response at $\mathbf{q} = 0$. In $Ba(Fe,Co)_2As_2$, finite $\mathbf{q}$ spin fluctuations can freeze and exhibit long range antiferromagnetism in vortex cores [50]. In FeSe we see no evidence for such behavior, which may be due to the presence of nematic order and the different contribution of orbital versus spin susceptibility. The absence of such fluctuations suggests that the high field phase is unrelated to SDW order [49, 51].

In summary, we find that the Knight shift is suppressed below T_c for in-plane fields, but see little to no suppression for field along the c-axis. The spectra are inhomogeneously broadened below T_c, and T_1^{-1} becomes frequency-dependent. These observations are consistent with a finite LDOS within the vortex cores. We find no evidence of competing antiferromagnetic fluctuations in the vortex cores. Further studies at higher fields or with Te doping should shed light on the unusual nature of the vortex states in this system.

[1] E. J. König and P. Coleman, Crystalline-symmetry-protected helical Majorana modes in the iron pnictides, Phys. Rev. Lett. **122**, 207001 (2019).

[2] P. Zhang, Z. Wang, X. Wu, K. Yaji, Y. Ishida, Y. Kohama, G. Dai, Y. Sun, C. Bareille, K. Kuroda, T. Kondo, K. Okazaki, K. Kindo, X. Wang, C. Jin, J. Hu, R. Thomale, K. Sumida, S. Wu, K. Miyamoto, T. Okuda, H. Ding, G. D. Gu, T. Tamegai, T. Kawakami, M. Sato, and S. Shin, Multiple topological states in iron-based superconductors, Nat. Phys. **15**, 41 (2018).

[3] L. Kong, L. Cao, S. Zhu, M. Papaj, G. Dai, G. Li, P. Fan, W. Liu, F. Yang, X. Wang, S. Du, C. Jin, L. Fu, H.-J. Gao, and H. Ding, Tunable vortex Majorana zero modes in LiFeAs superconductor, arXiv e-prints , arXiv:2010.04735 (2020), arXiv:2010.04735 [cond-mat.supr-con].

[4] Z. Wang, J. O. Rodriguez, L. Jiao, S. Howard, M. Graham, G. D. Gu, T. L. Hughes, D. K. Morr, and V. Madhavan, Evidence for dispersing 1d majorana channels in an iron-based superconductor, Science **367**, 104 (2020).

[5] Z. Wang, P. Zhang, G. Xu, L. K. Zeng, H. Miao, X. Xu, T. Qian, H. Weng, P. Richard, A. V. Fedorov, H. Ding, X. Dai, and Z. Fang, Topological nature of the FeSe$_{0.5}$Te$_{0.5}$ superconductor, Phys. Rev. B **92**, 115119 (2015).

[6] A. Kreisel, P. J. Hirschfeld, and B. M. Andersen, On the remarkable superconductivity of FeSe and its close cousins, Symmetry **12**, 1402 (2020).

[7] T. Hanaguri, S. Kasahara, J. Böker, I. Eremin, T. Shibauchi, and Y. Matsuda, Quantum vortex core and missing pseudogap in the multiband BCS-BEC crossover superconductor FeSe, Phys. Rev. Lett. **122**, 077001 (2019).

[8] T. Shibauchi, T. Hanaguri, and Y. Matsuda, Exotic superconducting states in FeSe-based materials, J. Phys. Soc. Japan **89**, 102002 (2020).

[9] S. Kasahara, Y. Sato, S. Licciardello, M. Čulo, S. Arsenijević, T. Ottenbros, T. Tominaga, J. Böker, I. Eremin, T. Shibauchi, J. Wosnitza, N. Hussey, and Y. Matsuda, Evidence for an fulde-ferrell-larkin-ovchinnikov state with segmented vortices in the BCS-BEC-crossover superconductor FeSe, Phys. Rev. Lett. **124**, 107001 (2020).

[10] P. O. Sprau, A. Kostin, A. Kreisel, A. E. Böhmer, V. Taufour, P. C. Canfield, S. Mukherjee, P. J. Hirschfeld, B. M. Andersen, and J. C. S. Davis, Discovery of orbital-selective cooper pairing in FeSe, Science **357**, 75 (2017).

[11] P. Bourgeois-Hope, S. Chi, D. Bonn, R. Liang, W. Hardy, T. Wolf, C. Meingast, N. Doiron-Leyraud, and L. Taillefer, Thermal conductivity of the iron-based superconductor FeSe: Nodeless gap with a strong two-band character, Phys. Rev. Lett. **117**, 097003 (2016).

[12] L. Jiao, C.-L. Huang, S. Rößler, C. Koz, U. K. Rößler, U. Schwarz, and S. Wirth, Superconducting gap structure of FeSe, Sci. Rep. **7**, 44024 (2017).

[13] P. K. Biswas, A. Kreisel, Q. Wang, D. T. Adroja, A. D. Hillier, J. Zhao, R. Khasanov, J.-C. Orain, A. Amato, and E. Morenzoni, Evidence of nodal gap structure in the basal plane of the FeSe superconductor, Phys. Rev. B **98**, 180501 (2018).

[14] F. Hardy, M. He, L. Wang, T. Wolf, P. Schweiss, M. Merz, M. Barth, P. Adelmann, R. Eder, A.-A. Haghighirad, and C. Meingast, Calorimetric evidence of nodal gaps in the nematic superconductor FeSe, Phys. Rev. B **99**, 035157 (2019).

[15] S.-H. Baek, D. V. Efremov, J. M. Ok, J. S. Kim, J. van den Brink, and B. Büchner, Orbital-driven nematicity in FeSe, Nat. Mater. **14**, 210 (2015).

[16] P. Wiecki, M. Nandi, A. E. Böhmer, S. L. Bud'ko, P. C. Canfield, and Y. Furukawa, NMR evidence for static local nematicity and its cooperative interplay with low-energy magnetic fluctuations in FeSe under pressure, Phys. Rev. B **96**, 180502 (2017).

[17] S.-H. Baek, D. V. Efremov, J. M. Ok, J. S. Kim, J. van den Brink, and B. Büchner, Nematicity and in-plane anisotropy of superconductivity in β-FeSe detected by ^{77}Se nuclear magnetic resonance, Phys. Rev. B **93**, 180502 (2016).

[18] J. Li, B. Lei, D. Zhao, L. Nie, D. Song, L. Zheng, S. Li, B. Kang, X. Luo, T. Wu, and X. Chen, Spin-orbital-intertwined nematic state in FeSe, Phys. Rev. X **10**, 011034 (2020).

[19] S. Molatta, D. Opherden, J. Wosnitza, Z. T. Zhang, T. Wolf, H. v. Löhneysen, R. Sarkar, P. K. Biswas, H. J. Grafe, and H. Kühne, Superconductivity of highly spin-polarized electrons in FeSe probed by ^{77}Se NMR, arXiv e-prints , arXiv:2010.10128 (2020), arXiv:2010.10128 [cond-mat.supr-con].

[20] K. Ishida, H. Mukuda, Y. Kitaoka, K. Asayama, Z. Q. Mao, Y. Mori, and Y. Maeno, Spin-triplet superconductivity in Sr$_2$RuO$_4$ identified by ^{17}O Knight shift, Nature **396**, 658 (1998).

[21] A. Pustogow, Y. Luo, A. Chronister, Y.-S. Su, D. A. Sokolov, F. Jerzembeck, A. P. Mackenzie, C. W. Hicks, N. Kikugawa, S. Raghu, E. D. Bauer, and S. E. Brown, Constraints on the superconducting order parameter in Sr$_2$RuO$_4$ from oxygen-17 nuclear magnetic resonance, Nature **574**, 72 (2019).

[22] V. Cvetkovic and O. Vafek, Space group symmetry, spin-orbit coupling, and the low-energy effective Hamiltonian for iron-based superconductors, Phys. Rev. B **88**, 134510 (2013).

[23] O. Vafek and A. V. Chubukov, Hund interaction, spin-orbit coupling, and the mechanism of superconductivity in strongly hole-doped iron pnictides, Phys. Rev. Lett. **118**, 087003 (2017).

[24] A. E. Böhmer, V. Taufour, W. E. Straszheim, T. Wolf, and P. C. Canfield, Variation of transition temperatures and residual resistivity ratio in vapor-grown FeSe, Phys. Rev. B **94**, 024526 (2016).

[25] S. I. Vedeneev, B. A. Piot, D. K. Maude, and A. V. Sadakov, Temperature dependence of the upper critical field of FeSe single crystals, Phys. Rev. B **87**, 134512 (2013).

[26] R. Zhou, D. D. Scherer, H. Mayaffre, P. Toulemonde, M. Ma, Y. Li, B. M. Andersen, and M.-H. Julien, Singular magnetic anisotropy in the nematic phase of FeSe, npj Quantum Materials **5**, 93 (2020).

[27] R. X. Cao, J. Hu, J. Dong, J. B. Zhang, X. S. Ye, Y. F. Xu, D. A. Chareev, A. N. Vasiliev, B. Wu, X. H. Zeng, Q. L. Wang, and G. Wu, Observation of orbital ordering and origin of the nematic order in FeSe, New J. Phys. **21**, 103033 (2019).

[28] K. R. Shirer, A. C. Shockley, A. P. Dioguardi, J. Crocker, C. H. Lin, N. apRoberts Warren, D. M. Nisson,

P. Klavins, J. C. Cooley, Y.-f. Yang, and N. J. Curro, Long range order and two-fluid behavior in heavy electron materials, Proc. Natl. Acad. Sci. **109**, E3067 (2012).

[29] D. M. Nisson and N. J. Curro, Nuclear magnetic resonance Knight shifts in the presence of strong spin-orbit and crystal-field potentials, New J. Phys. **18**, 073041 (2016).

[30] H. Kotegawa, S. Masaki, Y. Awai, H. Tou, Y. Mizuguchi, and Y. Takano, Evidence for unconventional superconductivity in arsenic-free iron-based superconductor FeSe: A ^{77}Se-NMR study, J. Phys. Soc. Japan **77**, 113703 (2008).

[31] N. Curro, T. Caldwell, E. Bauer, L. Morales, M. Graf, Y. Bang, A. Balatsky, J. Thompson, and J. Sarrao, Unconventional superconductivity in PuCoGa$_5$, Nature **434**, 622 (2005).

[32] S. Tan, Y. Zhang, M. Xia, Z. Ye, F. Chen, X. Xie, R. Peng, D. Xu, Q. Fan, H. Xu, J. Jiang, T. Zhang, X. Lai, T. Xiang, J. Hu, B. Xie, and D. Feng, Interface-induced superconductivity and strain-dependent spin density waves in FeSe/SrTiO3 thin films, Nat. Mater. **12**, 634 (2013).

[33] J. E. Sonier, Muon spin rotation studies of electronic excitations and magnetism in the vortex cores of superconductors, Rep. Progr. Phys. **70**, 1717 (2007).

[34] M. Abdel-Hafiez, J. Ge, A. N. Vasiliev, D. A. Chareev, J. V. de Vondel, V. V. Moshchalkov, and A. V. Silhanek, Temperature dependence of lower critical field H$_{c1}$(T) shows nodeless superconductivity in FeSe, Phys. Rev. B **88**, 174512 (2013).

[35] A. Maisuradze, R. Khasanov, A. Shengelaya, and H. Keller, Comparison of different methods for analyzing μSR line shapes in the vortex state of type-II superconductors, J. Phys.: Condens. Matter **21**, 075701 (2009).

[36] See Supplemental Material at [URL will be inserted by publisher] for [give brief description of material].

[37] A. Shi, T. Arai, S. Kitagawa, T. Yamanaka, K. Ishida, A. E. Böhmer, C. Meingast, T. Wolf, M. Hirata, and T. Sasaki, Pseudogap behavior of the nuclear spin–lattice relaxation rate in FeSe probed by ^{77}Se-NMR, J. Phys. Soc. Japan **87**, 013704 (2018).

[38] C. Caroli, P. D. Gennes, and J. Matricon, Bound fermion states on a vortex line in a type II superconductor, Phys. Lett. A **9**, 307 (1964).

[39] S. Dukan and Z. Tešanović, Superconductivity in a high magnetic field: Excitation spectrum and tunneling properties, Phys. Rev. B **49**, 13017 (1994).

[40] M. R. Norman, A. H. MacDonald, and H. Akera, Magnetic oscillations and quasiparticle band structure in the mixed state of type-II superconductors, Phys. Rev. B **51**, 5927 (1995).

[41] M. Ichioka, A. Hasegawa, and K. Machida, Field dependence of the vortex structure ind-wave ands-wave superconductors, Phys. Rev. B **59**, 8902 (1999).

[42] J.-X. Zhu, Local electronic structure in superconductors under a magnetic field, in *Bogoliubov-de Gennes Method and Its Applications* (Springer International Publishing, Cham, 2016) pp. 111–139.

[43] Y. Nakai, Y. Hayashi, K. Kitagawa, K. Ishida, H. Sugawara, D. Kikuchi, and H. Sato, Evidence of the bound states of the vortex state in ans-wave superconductor proved by NMR measurements, J. Phys. Soc. Japan **77**, 333 (2008).

[44] V. F. Mitrović, E. E. Sigmund, W. P. Halperin, A. P. Reyes, P. Kuhns, and W. G. Moulton, Antiferromagnetism in the vortex cores of YBa$_2$Cu$_3$O$_{7-\delta}$, Phys. Rev. B **67**, 220503 (2003).

[45] V. F. Mitrovic, E. E. Sigmund, M. Eschrig, H. N. Bachman, W. P. Halperin, A. P. Reyes, P. Kuhns, and W. G. Moulton, Spatially resolved electronic structure inside and outside the vortex cores of a high-temperature superconductor, Nature **413**, 6855 (2001).

[46] N. Curro, C. Milling, J. Haase, and C. Slichter, Local-field dependence of the O-17 spin-lattice relaxation and echo decay rates in the mixed state of YBa$_2$Cu$_3$O$_7$, Phys. Rev. B **62**, 3473 (2000).

[47] T. Imai, K. Ahilan, F. L. Ning, T. M. McQueen, and R. J. Cava, Why does undoped FeSe become a high-Tc superconductor under pressure?, Phys. Rev. Lett. **102**, 177005 (2009).

[48] S. Mukherjee, A. Kreisel, P. Hirschfeld, and B. M. Andersen, Model of electronic structure and superconductivity in orbitally ordered FeSe, Phys. Rev. Lett. **115**, 026402 (2015).

[49] N. Zhou, Y. Sun, C. Y. Xi, Z. S. Wang, Y. F. Zhang, C. Q. Xu, Y. Q. Pan, J. J. Feng, Y. Meng, X. L. Yi, L. Pi, T. Tamegai, X. Xing, and Z. Shi, Disorder-robust high-field superconducting phase of FeSe single crystals, arXiv e-prints , arXiv:2102.02353 (2021), arXiv:2102.02353 [cond-mat.supr-con].

[50] J. Larsen, B. M. Uranga, G. Stieper, S. L. Holm, C. Bernhard, T. Wolf, K. Lefmann, B. M. Andersen, and C. Niedermayer, Competing superconducting and magnetic order parameters and field-induced magnetism in electron-dopedBa(fe1-xCox)2as2, Physical Review B **91**, 024504 (2015).

[51] B. L. Young, R. R. Urbano, N. J. Curro, J. D. Thompson, J. L. Sarrao, A. B. Vorontsov, and M. J. Graf, Microscopic evidence for field-induced magnetism in CeCoIn$_5$, Phys. Rev. Lett. **98**, 036402 (2007).

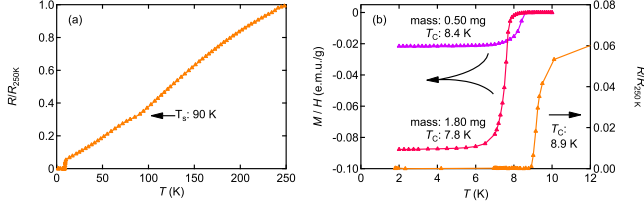FIG. 5. (a) Temperature dependent resistivity curve showing the structural transition, $T_s \approx 90\,\mathrm{K}$ and a $T_c = 8.9\,\mathrm{K}$. (b) A zoom in showing the superconducting transition with magnetic susceptibility (purple and red curves) and resistivity (orange curve) data.

SUPPLEMENTAL INFORMATION

Sample Characteristics

Single crystals of FeSe were grown using a vapor transport technique with an angled two-zone furnace [24]. Single crystal samples were characterized via resisitivity and magnetic susceptibility measurements (Fig. 5). The resistivity data (R/R_{250K}) clearly shows the structural transition $T_s \approx 90\,\mathrm{K}$ and has a superconducting transition $T_c = 8.9\,\mathrm{K}$. These temperatures and a residual resistivity ratio (RRR_{250K}) value (18.8) show that our samples are of similar quality to the ones previously reported. As first noted by Böhmer, the offset of resistivity superconducting transition corresponds well with the initial downturn of the magnetic susceptibility. We also note that we found a slight inverse relationship between sample size and transition temperature (Fig. 5(b)). This relationship combined with the slight oxidation of storing the sample in an Ar-glovebox for a year explains the slightly lower superconducting transition of the sample measured in NMR.

Knight shift at Different Power Levels

The left panel of Fig. 6 shows the Knight shift versus temperature for different power levels. In the first case, the spectra were measured at high power and there is no obvious change below T_c due rf heating effects. At low power, the shifts are reduced in the superconducting state.

Vortex Lineshape and Knight shift Inhomogeneity

Figure 7 compares the spectrum in the normal and superconducting state for $\mathbf{H}_0 \parallel [110]$. In order to model the lineshape in the mixed phase, we use a Monte Carlo approach to compute the histogram, $P(f)$, of local res-
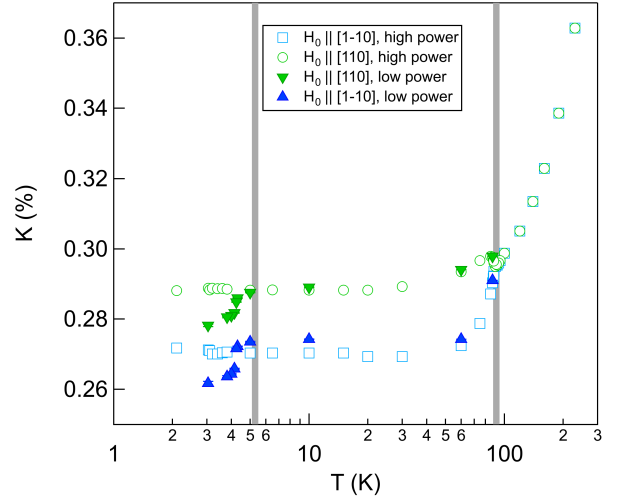

FIG. 6. (Knight shifts along the a and b directions measured at low and high power. The reduction below T_c is only evident with low power pulses, such that there is no Joule heating of the sample. Differences in the shift above T_c between high and low power spectra are due to slightly worse alignment with $[110]/[1\bar{1}0]$ for the low power spectra.

onance frequencies in a hexagonal vortex lattice, where the frequency is given by $f(\mathbf{r}) = \gamma B(\mathbf{r})(1 + K(\mathbf{r}))$. The local field is given by the London model with a Gaussian cutoff [35]:

$$B(\mathbf{r}) = H_0 \sum_{\mathbf{G}} \frac{e^{-i\mathbf{G}\cdot\mathbf{r}}}{1 + (\lambda \cdot \mathbf{G})^2} e^{-|\mathbf{G}|^2 \xi^2/2}, \qquad (1)$$

$\mathbf{G}$ are the reciprocal lattice vectors for a hexagonal vortex lattice, $\lambda = (\lambda_a, \lambda_c)$ with $\lambda_a = 446$ nm, $\lambda_c = 1320$ nm, and $\xi = 3.1$ nm [34]. If we assume that $K(\mathbf{r}) = 0$, then $P(f)$ is given by the green curve in Fig. 7. Although this spectrum does have a high frequency tail, it remains too small to explain the observed inhomogeneity.

To model the spatial dependence of $K(\mathbf{r})$, we assume that it exhibits the periodicity of the vortex lattice with maxima within the cores and vanishing outside, with the expression:

$$K(\mathbf{r}) = \delta K \sum_{G} e^{-|\mathbf{G}|^2 \xi^2/2} \left(e^{-i\mathbf{G}\cdot\mathbf{r}} - e^{-i\mathbf{G}\cdot\mathbf{r}_0} \right)/K_0, \quad (2)$$

where $K_0 = \sum_{\mathbf{G}'} \exp(-|\mathbf{G}'|^2 \xi^2/2)\left(1 - e^{-i\mathbf{G}'\cdot\mathbf{r}_0}\right)$, $\mathbf{r}_0 = \{a/2, \sqrt{3}a/6\}$ is the location of the field minimum between the vortex cores, a is the unit cell length for the hexagonal vortex lattice, and δK is the shift within the cores. This distribution is illustrated in the inset of Fig. 7 for $\delta K = 100$ ppm. In this case, $P(f)$, shown in blue in Fig. 7, is broader and the high frequency tail is extended up to the normal state resonance frequency.
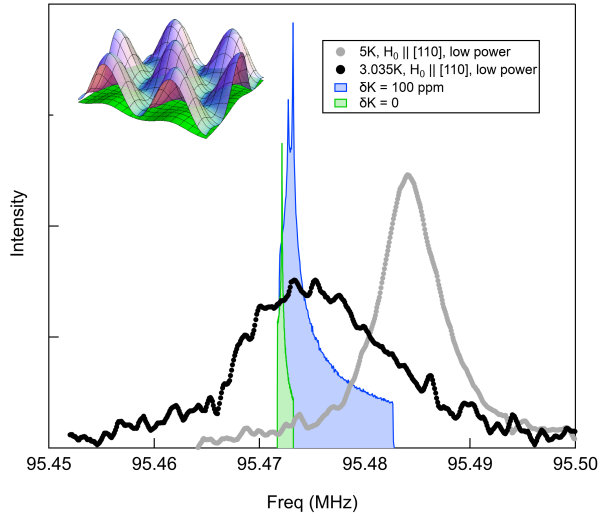
FIG. 7. ^{77}Se NMR spectra in the normal and superconducting states at 12 T, measured at low power for field along the [110] direction. The solid green and blue regions indicate the theoretical spectra computed for a vortex lattice with and without a finite Knight shift, δK, in the cores, respectively, as discussed above. The inset shows how the resonance frequency varies as a function of position with and without δK.